Soft Matter

Dynamic Article Links

Cite this: *Soft Matter*, 2012, **8**, 1673

www.rsc.org/softmatter

PAPER

Surface energy tunable nanohairy dry adhesive by broad ion beam irradiation

Yudi Rahmawan,[ab] Tae-il Kim,[c] Seong Jin Kim,[b] Kwang-Ryeol Lee,[b] Myoung-Woon Moon*[b] and Kahp-Yang Suh*[a]

Received 24th August 2011, Accepted 25th November 2011
DOI: 10.1039/c2sm06614a

We present a simple and shape-controllable method to tune the surface energy and tilting angle of nanohairy structures using broad ion beam irradiation. First, the vertical nanohair arrays made of ultraviolet (UV)-curable polyurethane acrylate (PUA) material were prepared by replica molding. Subsequently, the nanohairs were bent to a wide range of angles from 0 (vertical) to 75° (stooped hairs) by the oblique broad Ar ion beam. The surface energy was tuned with normal oxygen (O_2) ion beam irradiation together with aging effect (47.1 to 71.9 mJ m^{-2}). It was observed that the shear adhesion strength was significantly increased from 25.2 to 58.1 N cm^{-2} on the hydrophilic test surface and from 22.8 to 45.7 N cm^{-2} on the hydrophobic test surface, respectively, with the variation of surface energy from 47.1 to 71.9 mJ m^{-2}. In addition, the shear adhesion strength was increased from 58.1 to 124.1 N cm^{-2} and from 45.7 to 110.6 N cm^{-2} on hydrophilic and hydrophobic test surfaces, respectively, as the tilting angle was varied from 0 to 75° at the highest surface energy of 71.9 mJ m^{-2}. The measured adhesion data were compared with the theoretical adhesion forces based on Johnson–Kendall–Roberts (JKR), modified-JKR, peel zone (PZ), and Kendall peeling models, suggesting that the contact state of nanohairs is a mixture of tip and side contacts.

Introduction

Since the discovery of the adhesive mechanism of a single gecko foot-hair, there has been significant achievement towards understanding the role of hierarchy and leaning angle of micro- and nanohairs.[1–7] With these structural features, the gecko lizard has the ability to cling to almost all kinds of surfaces regardless of roughness and angle like wall or ceiling as well as to detach effortlessly from the surfaces with a speed of >1 m s^{-1} and self-clean its pads. It has also been revealed that the governing force in the gecko-inspired dry adhesion system is determined mainly from the contact geometry of hairs (tip shape, hair density, preload, *etc.*)[8–16] and environmental conditions (temperature, humidity, *etc.*).[17–22] In particular, multiscale hairs on a gecko's foot in the form of seta or spatula were found to be tilted for optimized motion with directional anisotropy in the attachment and detachment directions.

To exploit the above structural features, many research groups have demonstrated several artificial dry adhesives based on polymer materials, but their efforts have been mostly focused on tuning the geometrical parameters such as tip shape, tilting angle, aspect ratio, *etc.* Due to recent advances in micro- and nano-fabrication methods, it is now possible to achieve higher adhesion strength than that of the gecko foot hair (~10 N m^{-2}) by several times. To the best of our knowledge, the maximum value of polymer-based dry adhesive was reported to be 26 N m^{-2} using tilted nanohairs with the density of 1.3×10^8 hairs cm^{-2}.[23,24]

A handful of works have been reported to date for industrial applications concerning the enhancement of surface energy.[25,26] However, there has been no trial to modulate the surface energy of nanohairs to elevate the strength of dry adhesion. Here, we demonstrate that both the geometry and surface chemistry can be orchestrated so as to tune the shear adhesion strength of tilted nanohair arrays. For the fabrication, broad Ar ion beam irradiation was utilized to tilt the nanohairs to a certain angle over a large area. Subsequently, surface energy was controlled *via* oxygen ion beam irradiation on vertical and tilted nanohairs. As a result, the surface energy was modified in the range of 47.6 to 71.9 mJ m^{-2} for various tilting angles from 0 (vertical) to 75° (stooped hairs). It is noted that the maximum adhesion strength of 124.1 N cm^{-2} was achieved for the nanohairs with the tilting angle of 75° and surface energy of 71.9 mJ m^{-2}, which was more than 10 times higher than that of real gecko adhesion strength.

We first fabricated nanohair arrays with various surface energies by employing a replica molding process of a UV-curable polyurethane acrylate (PUA) material (Young's modulus: 20 MPa) and O_2 ion beam irradiation process. As schematically illustrated in Fig. 1(a), well-defined nanohair arrays of 100 nm

[a]*WCU Program on Multiscale Mechanical Design, School of Mechanical and Aerospace Engineering, Seoul National University, Gwanak-1, Gwanak-ro, Gwanak-gu, Seoul, 151-742, Korea. E-mail: sky4u@snu.ac.kr; Fax: +82-2-883-0179; Tel: +82-2-880-9103*
[b]*Future Convergence Research Division, Korea Institute of Science and Technology, Hwarang-ro14-gil 5, Seongbuk-gu, Seoul, 136-791, Korea. E-mail: mwmoon@kist.re.kr; Fax: +82-2-958-5509; Tel: +82-2-958-5487*
[c]*3014 Materials Research Laboratory, University of Illinois at Urbana-Champaign, 104 S Goodwin Ave, Urbana, IL, 61801, USA*

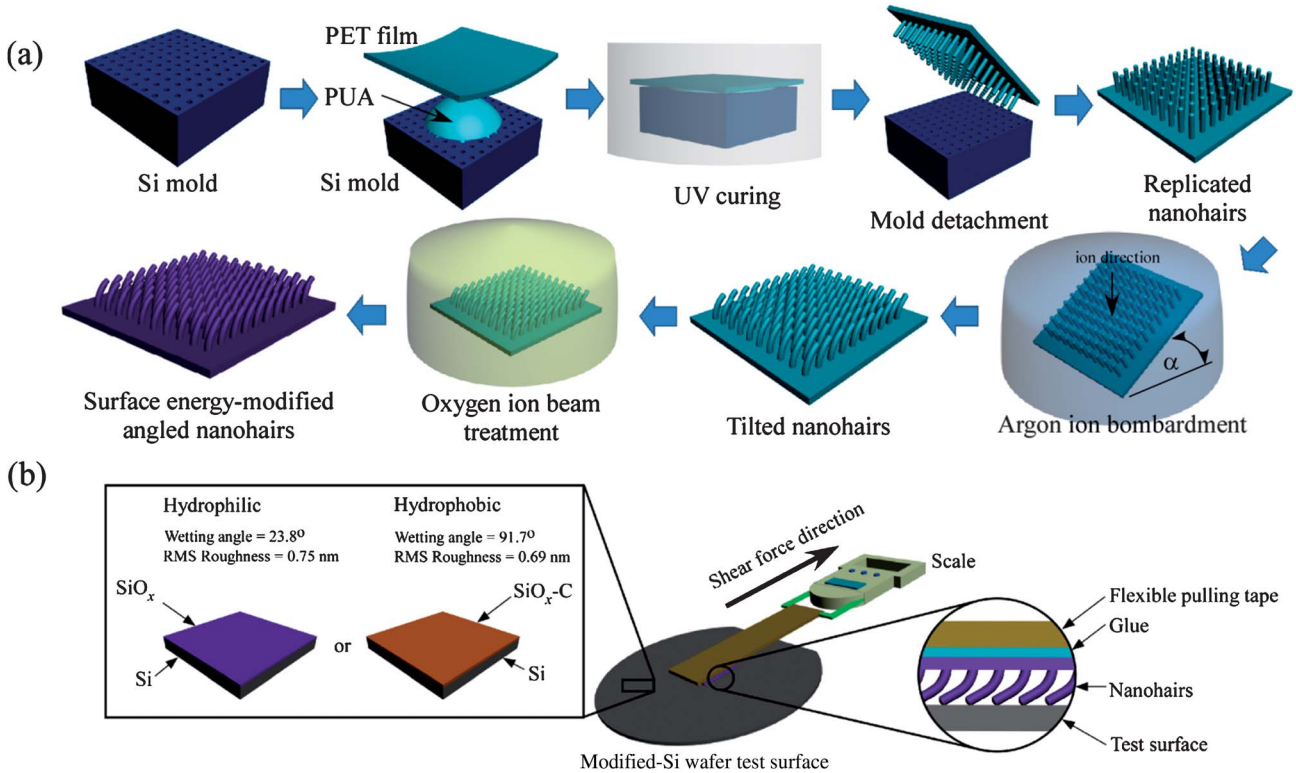

Fig. 1 (a) Fabrication of tilted nanohair arrays with surface energy modification and (b) experimental setup for measuring macroscopic shear adhesion force on hydrophilic (SiO_x) and hydrophobic (SiO_x–C) test surfaces.

diameter and 1 μm height (aspect ratio = 10) were replicated from the silicon master that had been prepared by photolithography and reactive ion etching. Subsequently, the as-formed nanohairs were irradiated by Ar ion beam at a tilting angle (0–90°). The leaning angle was controllable by changing the incident angle of ion beam against the nanohair with a constant exposure time of 1 min. It is noted that such an oblique ion beam treatment was capable of completing structure transformation in a more rapid and scalable manner, as compared to the oblique e-beam irradiation demonstrated earlier.[27,28]

For hydrophilic surface treatment, the irradiated nanohairs were further exposed to O_2 ion beam at the normal incident angle for 30 s in order to minimize the possible etching effect on the surface. The treatment then gave rise to a dramatic enhancement of surface energy from 21.3 to 71.9 mJ m^{-2}. As time goes by, the surface energy was gradually decreased in the course of recovering its initial pristine state due to well-known hydrophobic recovery by bond breakage and environmental carbon species. Such an aging effect refers to a continuous conversion of the hydrophilic surface into a pristine hydrophobic surface with time,[29] which allows for a simple way of modulating the surface energy within a certain range.

To study the effect of surface energy and tilting angle of nanohairy structures, the macroscopic shear adhesion force was measured using the hanging scales method on two different counter surfaces: hydrophilic- and hydrophobic-modified Si wafers (Fig. 1(b)). The hydrophobic test surface (wetting angle: 91.7 ± 4.7°) was prepared by depositing a 45 nm thick layer of polymeric SiO_x-incorporated diamond-like carbon (DLC) using a conventional chemical vapour deposition (CVD) process.[30,31] The hydrophilic test surface was a pristine Si ⟨100⟩ wafer with native oxide (wetting angle: 23.8 ± 2.3°). Then, the adhesion force was measured on a set of vertical nanohairy samples with variation in the surface energy from 47.6 to 71.9 mJ m^{-2} and a set of samples having the highest surface energy (71.9 mJ m^{-2}) with variation in the tilting angle from 0 to 75°.

Materials and method

Fabrication of vertical nanohair arrays by replica molding

A Si master was prepared by conventional photolithography and reactive ion etching, which contained high-density hole arrays of 100 nm diameter and 1 μm height (aspect ratio = 10). The nanohairs were equally spaced at a distance of 100 nm and the patterned field was 3 × 3 cm^2, giving a hair density of 6.16 × 10^8 cm^{-2}. Then, a UV-curable PUA precursor (RM301, Minuta Tech, Korea, Young's modulus: 20 MPa) was drop-dispensed onto the Si master. A thin polyethylene terephthalate (PET) sheet (thickness: 50 μm) was subsequently placed and squeezed gently to spread the PUA precursor on the Si master uniformly. The assembly was cured under UV of 100 W cm^{-2} dose (Fusion Cure System, Minuta Tech, Korea) for 23 s. The cured PUA was peeled off from the Si master, resulting in a positive copy of nanohair arrays with respect to the original master.

Fabrication of geometry-controllable, tilted nanohair arrays with various surface energies

An end-Hall type linear ion gun system (Alcatel Vacuum Technology, France) was used to irradiate Ar and O_2 ion beams on

the as-formed nanohair arrays. First, Ar irradiation was performed to transform straight nanopillars into tilted ones with a tunable leaning angle. Specifically, the sample was put in the chamber and the air was evacuated to a base pressure of 2×10^{-5} mbar. The anode voltage during ion treatment was kept constant at 1 keV with a current density of 50 μA cm^{-2} and a Radio Frequency (RF) bias voltage of −600 V was applied to the sample holder.[32] The Ar gas was introduced from the pure gas source at a flow rate of 8 sccm and the ion beam was directionally irradiated at a tilting angle from 0 to nearly 90° with a fixed treatment time of 1 min. The ion beam incident angle was varied by tilting the sample holder against the ion beam incident direction. After tilting the nanohairy structure, the oxygen ion treatment was subsequently performed to increase the surface energy of the tilted nanohairy structures. Oxygen ion beam treatment was done with normal direction of the sample surfaces for 30 s, which turned out to be optimal to avoid mechanical erosion by excessive ion irradiation. With such a low irradiation energy as small as 1 keV, which is roughly 1/10 of that used in the previous work,[33] the effective modulus was not changed significantly. The overall process is drawn schematically in Fig. 1(a).

Surface characterization

The surface energy was measured using the Owens–Wendt method with de-ionized (DI) water and formamide as two probing liquids.[34] All contact angle (CA) measurements were done using a contact angle analyzer (KRUSS DSA 100, Germany) on idealized flat surfaces with sessile droplet mode. The PUA flat surfaces were made by replication of PUA from Si ⟨100⟩ wafer. After the identical surface treatment with nanohairy structures, the surface energy of the flat PUA surface was calculated by measuring CAs over at least three different locations and an average value was used for the plot and calculation. The contact angle hysteresis (CAH) was determined by the measurement of advancing and receding CAs on the surfaces. The continuous mode of water dispensing and retracting was done with the speed of 10 μl min^{-1} using the same apparatus.

Detailed images of nanohairy structures were taken using a scanning electron microscope (SEM, NanoSEM 200, FEI Company, USA). An accelerating voltage of 10 kV was used during observation and the surface was coated with a thin Pt layer to a thickness of 8 nm to prevent electron charging. The X-ray photoelectron spectroscopy (XPS) measurements were performed with a PHI 5800 ESCA system (Physical Electronics) using Al Kα radiation ($h\nu = 1486.6$ eV).

Measurement of shear adhesion strength

The macroscopic shear adhesion force was measured by a pulling test with a custom-built device (see details in Fig. 1(b)). The shear adhesion force was translated into shear adhesion strength by multiplying individual force in each nanohair with the total number of hairs per unit area. Here a hanging scale with precision of ±20 g (Kern and Sohn GmbH, Germany) was used to pull the samples of well-aligned pillar arrays against hydrophobic and hydrophilic surfaces of Si ⟨100⟩ wafer (Silicon Materials Inc., USA), which were used as representative counter surfaces with the nanohairs. The RMS surface roughness of the two test surfaces was measured to be 0.69 ± 0.23 and 0.75 ± 0.2 nm, respectively, using atomic force microscopy (AFM, SIS Nanostation II, Germany) scanning on an area of 30 μm × 30 μm. The nanohairy surface was manually placed on the testing surface with a 300 g pre-load to ensure an initial uniform contact. The measurement was done at a room temperature of ~26.3 °C with a relative humidity of 57.1 ± 6.6%.

Results and discussion

Tuning the surface energy and tilting angle of nanohairs

Fig. 2(a) shows tilted SEM images of the as-formed and irradiated nanohair arrays at different incident angles of 30, 45, and 75°, respectively. In the Ar ion beam treatment, the exposure time was fixed at 1 min to minimize mechanical erosion of the nanohairs under excessive ion irradiation on the side of the hairy structure. As reported earlier, the bending mechanism is associated with the stiffening process as well as local shrinkage on the ion beam exposed polymer surface.[32] Therefore, the nanohairs were bent towards the incident direction of ion beam. By considering that the penetration depth of the affected surface would be determined mainly by the accelerating voltage,[35] a relatively low voltage (1 keV) was used in our experiment, which is much lower than that used in our previous work (10–50 keV).[33] The estimated penetration depth of the affected surface in our samples was approximately 3.5 nm. Therefore, the apparent Young's modulus of nanohairs would not be affected significantly by the irradiation process. As can be seen from Fig. 2(b), the tilting angle of nanohairs, β, as defined in the inset, can be controlled by the incident angle of ion beam, α. It is noted that two different morphologies were observed depending on α. At lower α (<60°), the nanohairs showed a relatively straight shape due to the full exposure of the body of the nanohair structure to ion beam irradiation. At higher α (>60°), on the other hand, the upper part of nanohairs was more tilted towards the beam direction probably due to a shadowing effect, *i.e.*, the lower part was not fully exposed to the beam. For this reason, the tilting angle is characterized by an exponential increase as a function of α.

Next, the surfaces of vertical and tilted nanohairs were modified to hydrophilic by exposure to O_2 ion beam irradiation and a subsequent hydrophobic recovery process.[36,37] In order to determine the surface energy of PUA surfaces with O_2 ion beam treatment and aging, CAs of two probing liquids (DI water and formamide) were measured and each surface energy value was derived according to the Owens–Wendt (O–W) method.[34] According to previous reports,[38,39] the measurement error in the O–W method is considerably small, typically not exceeding 3% over the range of 20–50 mJ m^{-2} on most of the polymeric surfaces. In the case of high energy surfaces such as metals or inorganic materials, however, an advanced method such as the acid–base method with three probing liquids needs to be employed.

Fig. 3 shows the changes of surface energy and various CAs on flat and structured PUA surfaces with or without ion beam treatment. It is clearly seen from Fig. 3(a) that the surface energy of a pristine PUA sample (21.3 mJ m^{-2}) was dramatically increased to 71.9 mJ m^{-2} after oxygen ion beam treatment. As time goes by, the surface energy of nanohairs gradually decreased to

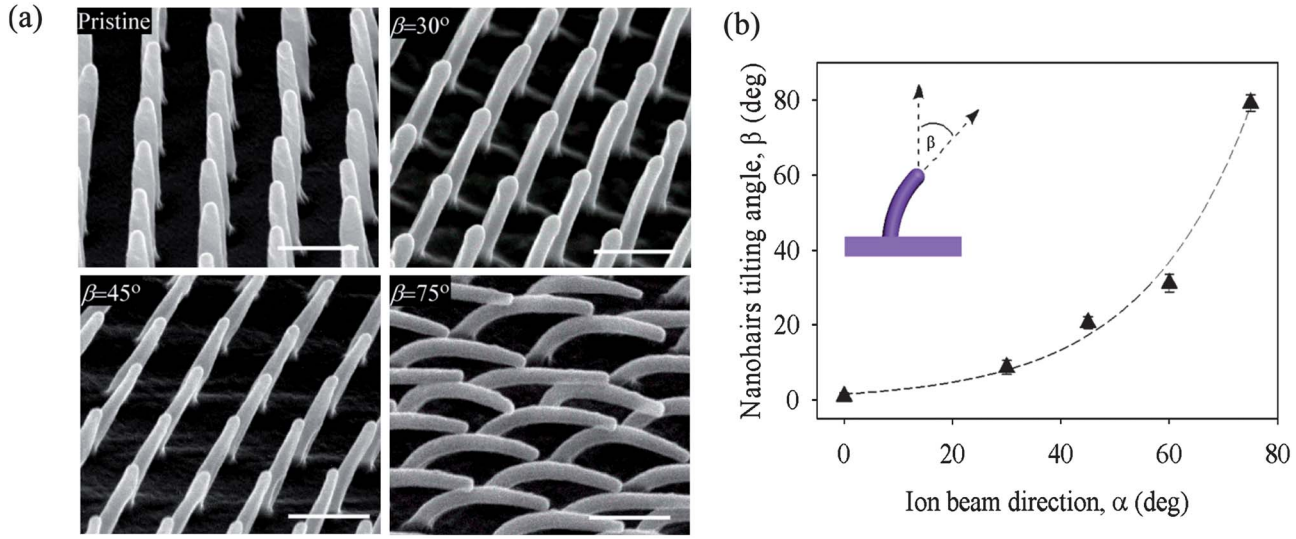

Fig. 2 (a) SEM images (45° tilting view) showing pristine nanohairs array and Ar-irradiated nanohair arrays with different tilting angles, β. Unlike other hairy structures, the upper part is highly bended in the case of 75°, which shows the highest shear adhesion due to an enhanced side contact. Scale bar is 500 nm. (b) The change of tilting angle (β) as a function of Ar ion beam incident angle (α) for a fixed irradiation time of 1 min. The dashed line is for guiding eyes. The inset shows the definition of tilting angle.

47.6 mJ m^{-2} for the duration of 30 days under ambient conditions (temperature: 26.3 °C, relative humidity: 57.1 ± 6.6%) (see Table 1). It is worthwhile to note that the surface energy of the aged PUA surface did not reach the original state of the pristine PUA surface for 30 days, suggesting that some permanent modification had occurred by O_2 ion beam treatment. Fig. 3(b) and (c) shows the advancing, receding, and static CAs on flat and nanohairy PUA surfaces with aging time. On both surfaces, the CAH turned out to be nearly zero right after the oxygen ion beam treatment, gradually increased to ~20° after aging for 5 days, and almost unchanged thereafter. The difference between the advancing and static CAs was quite small, suggesting that both CAs could represent the lowest energy state. It is interesting to note that the CAH has a direct relation with the surface energy or the adhesion strength of the surfaces. On hydrophilic materials, when the surface energy was decreased (*i.e.*, decrease of adhesion strength), the CAH was increased. This observation was valid both on flat and nanohairy PUA surfaces. In order to decouple the effect of geometry and surface treatment, we have investigated the role of nanohairy geometry in terms of tilting angle as shown in Fig. 3(d). Here, the CAH was measured on a pristine, chemically non-modified nanohairy PUA surface with different tilting angles. As shown, the CAH was decreased with the increase of tilting angle (*i.e.*, increase of adhesion energy). Taken together, we suggest that the CAH can be used as a measure to predict the adhesion strength in such a way that the CAH is inversely proportional to the adhesion strength for flat and structured surfaces.

Comparison of adhesion strength with theoretical models

To explain the measured adhesion strength in terms of surface energy and geometry, we use a simple theory based on Fowkes' additivity of intermolecular forces at the interface.[40] We hypothesize that the effect of surface energy can be incorporated into the variation of work of adhesion, which in turn gives a direct change into the adhesion strength of hairy structures. As is well known, the work of adhesion is the energy required to separate objects into two surfaces. Based on Fowkes' theory of additivity, the interfacial energy, γ_{12} is the sum of polar and non-polar (dispersive) components:[40,41]

$$\gamma_{12} = \gamma_1 + \gamma_2 - W_{12}^{p} - W_{12}^{d}. \quad (1)$$

Here γ is the surface energy and W is the work of adhesion. The subscripts 1, 2 and superscripts p, d refer to objects 1, 2 and polar and dispersive components, respectively. From this equation, one can determine the dependency of work of adhesion on surface energy. Wu found that the work of adhesion can be calculated from surface energies of polar and non-polar terms:[41]

$$W_{12} = 2[(\gamma_1^{d}\gamma_2^{d})^{0.5} + (\gamma_1^{p}\gamma_2^{p})^{0.5}]. \quad (2)$$

a. Effect of surface energy. In order to estimate the adhesion strength of vertical nanohairs, we compare two extreme cases of tip and side contacts due to an applied shear force-induced bending. For the tip contact at the nanohair interface, we employ the well-established Johnson–Kendall–Roberts (JKR) theory between elastic spheres, which has been widely used to estimate the theoretical adhesion force of gecko-inspired dry adhesives.[4,12,42] Here, the spatula of the gecko foot is assumed to be an elastic sphere of radius r, where the total adhesion force is given by $F_{JKR} = (3/2)\pi r W_{12}$.[43] Accordingly, the variation of surface energy directly changes the work of adhesion in such a way that the total adhesion strength is increased with the increase of surface energy. This model can be used as the lower boundary of the estimated adhesion strength as it calculates the adhesion strength based on the tip contact of each nanohair.

During dynamic application of shear force, the vertical and pre-tilted hairs can be easily bent to form a side contact to the

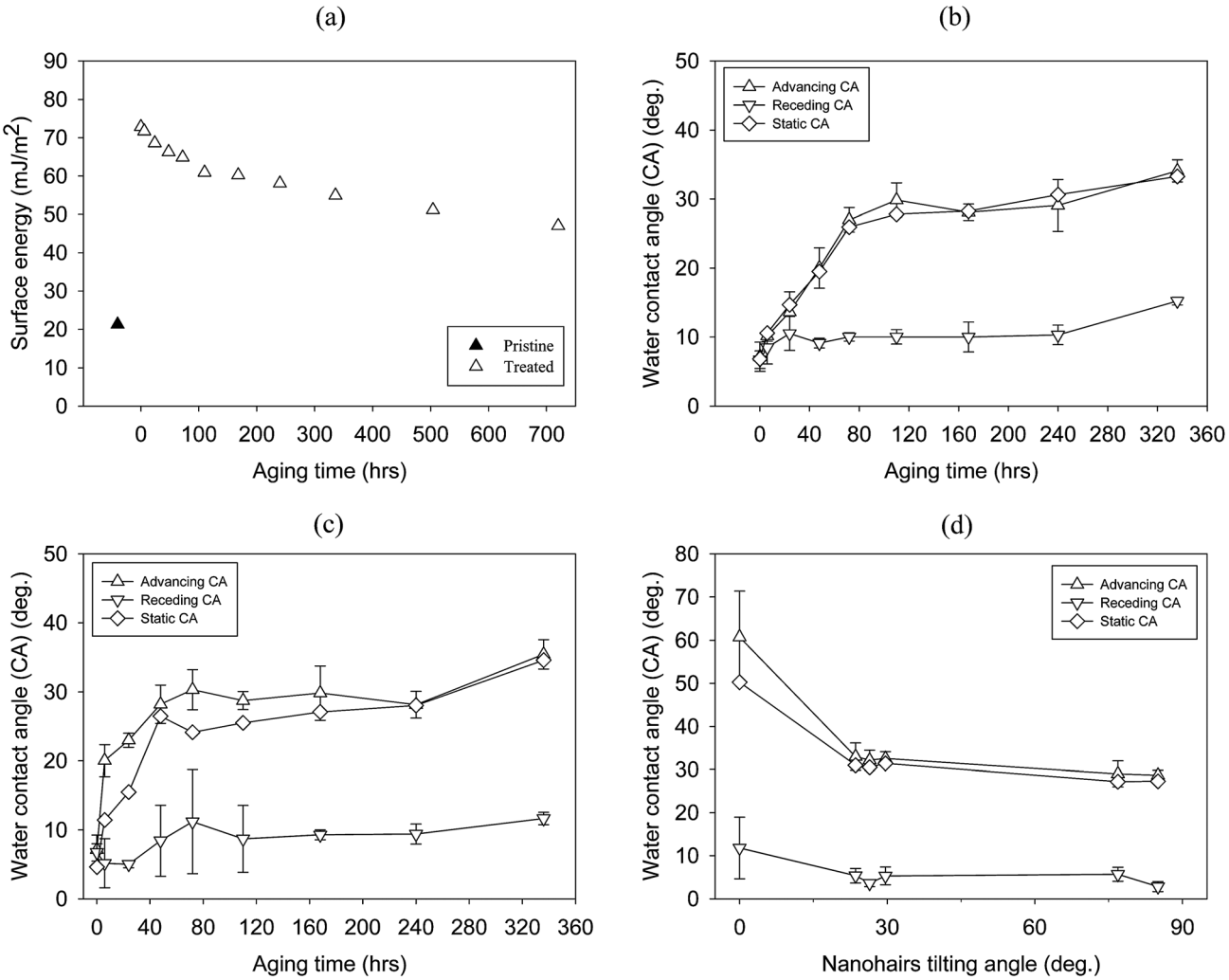

Fig. 3 Plots showing the changes of surface energy and CAs after chemical and geometry modification. (a) The plot of surface energy after ion beam irradiation with aging time. (b–d) The plots of advancing, receding, and static CAs of (b) flat PUA surfaces after ion beam irradiation, (c) nanohairy surfaces after ion beam irradiation, and (d) chemically non-modified PUA nanohairy surfaces with different nanohair tilting angles.

Table 1 Surface energy and atomic composition (from XPS spectra) with aging time for pristine and oxygen-irradiated samples

Aging time after O_2 ion beam treatment (days)	Surface energy/mJ m^{-2}	Atomic composition (at.%)			
		C	Si	O	N
Pristine[a]	21.3 ± 0.9	57.18	12.05	30.1	0.67
0	71.9 ± 0.3	44.62	10.72	43.57	1.1
7	60.2 ± 1.5	49.07	10.3	39.53	1.1
30	47.6 ± 1.1	47.84	12.53	38.94	0.69

[a] Pristine sample is the one with vertical nanohairs without O_2 ion beam treatment.

flat surface. Therefore, we use the modified-JKR model for side contact of a cylindrical soft object to a flat solid surface.[44] Here, the adhesion force of a single hair is given by[44] $F_{\text{Mod-JKR}} = 3.16(KW_{12}^2 r)^{1/3} L_c$. Here, $K = 4E^*/3$ where $1/E^* = (1 - \upsilon_1^2)/E_1 + (1 - \upsilon_2^2)/E_2$. E and υ with subscripts 1 and 2 are the Young's modulus and Poisson's ratio of objects 1 and 2, respectively. Assuming that a single nanohair is an elastic rod, the side contact length ($L_c = L - L_a$) for a given shear load (f_s) acting on the tip of a nanohair can be obtained by solving the differential equation:[45,46] $\varphi'' + (f_s/EI)\cos\varphi = 0$ with the corresponding boundary conditions of $\varphi(0) = \varphi_i$; $\varphi(a) = \pi/2$; and $\varphi(a) = \sqrt{(2\omega_{12}/EI)}$. Here L is the total length of a nanohair, L_a is the distance of initial contact on a nanohair, φ is the tilting angle of a nanohair, I is the moment of inertia of a nanohair and ω_{12} is the adhesion energy per length, which is given by:[47,48]

$$\omega_{12} = 6\left\{\frac{(1-\upsilon^2)r^2 W_{12}^4}{\pi E}\right\}^{1/3}. \quad (3)$$

With the solution of L_a,[46] we plotted the corresponding maximum contact length as a function of surface energy and tilting angle of nanohairs as shown in Fig. 4(a) and (b). It is noted that the estimated contact length increased almost linearly with the variation of surface energy and tilting angle of nanohairs: it was varied from 576 to 668 nm and 496 to 620 nm for hydrophilic and hydrophobic counter surfaces, respectively, with the corresponding change of surface energy for vertical nanohairs from 47.6 to 71.9 mJ m^{-2}.

With all known components of the JKR and modified-JKR for side contact models, the theoretical shear adhesion strength for vertical nanohairs can be calculated as shown in Fig. 5(a). As can be seen from the figure, a trend of linear increase was observed from the theoretical predictions on both hydrophilic and hydrophobic surfaces, whereas the experimental data showed a slight exponential increase with the surface energy. The JKR model with the low estimation of adhesion strength can be used as a lower bound of theoretical adhesion as it involves tip contact of nanohairs. Similarly, the modified-JKR with side contact model can provide an upper bound as it idealizes a uniform contact of an individual hair on a flat surface. Therefore, it can be said that the actual contact consists of a composite state of the two extreme cases where an exact contribution from each contact condition might be associated with the dynamic shear force application and hair geometry. The fact that the experiment and theory show the similar trends with the change of surface energy suggests that the role of surface energy is well represented in both theoretical models. It appears that the dynamic shearing force during shear force test makes a portion of vertical pillars tilted, resulting in a moderate side contact of hairs with the surface.

b. Effect of tilting angle. When a thin elastic solid in contact with a rigid substrate is peeled with a certain angle of θ from the surface, the peeling force can be dominated by the elastic term instead of surface energy and potential energy terms.[49] The model has been applied to biological attachment during locomotion.[50] According to the Kendall peeling model, the peeling force is expressed as a function of peeling angle (θ) by $F/b = R/(1 - \cos\theta)$ where b is the contact width and R is the adhesive energy.

Alternatively, Pesika *et al.* have proposed the peel zone (PZ) model with an angle-dependent multiplier on the same system where the peeling force can be calculated from:[51]

$$\frac{F}{b} = \frac{2R\theta}{\pi(1-\cos\theta)\sin\theta}. \quad (4)$$

The theoretical adhesion strength based on the Kendall peeling and PZ models is displayed in Fig. 5(b) along with the experimental data, indicating that the calculated adhesion strength was increased from nearly zero in the peeling direction of 90° and increased enormously as the peeling angle approaches 0° (or lap shear joint). The peeling angle-dependent multiplier gives a smaller value in the PZ model compared to the Kendall peeling model due to the increase of the peel zone with the decrease of the peeling angle.

Using the modified-JKR model for side contact, one can also predict the adhesion strength of tilted nanohairs. Here, the contact length, L_c, is a function of effective elastic modulus for the tilted nanohairs and the effective elastic modulus is given by[52]

$$E_{\text{eff}} = \frac{3EID\sin\beta}{L^2\cos^2\beta[1 \pm \mu\tan\beta]}, \quad (5)$$

where D is the density and μ is the friction coefficient of a nanohair.

When the tilting angle was varied from 0 to 75° with the constant surface energy of 71.9 mJ m^{-2}, the theoretical contact length turned out to be even longer: it ranged from 668 to 747 nm and 620 to 706 nm for hydrophilic and hydrophobic counter surfaces, respectively. The reason can be attributed to the increased contact length with reduced effective elastic modulus in the solution of side contact length described previously (see Fig. 4(b)).

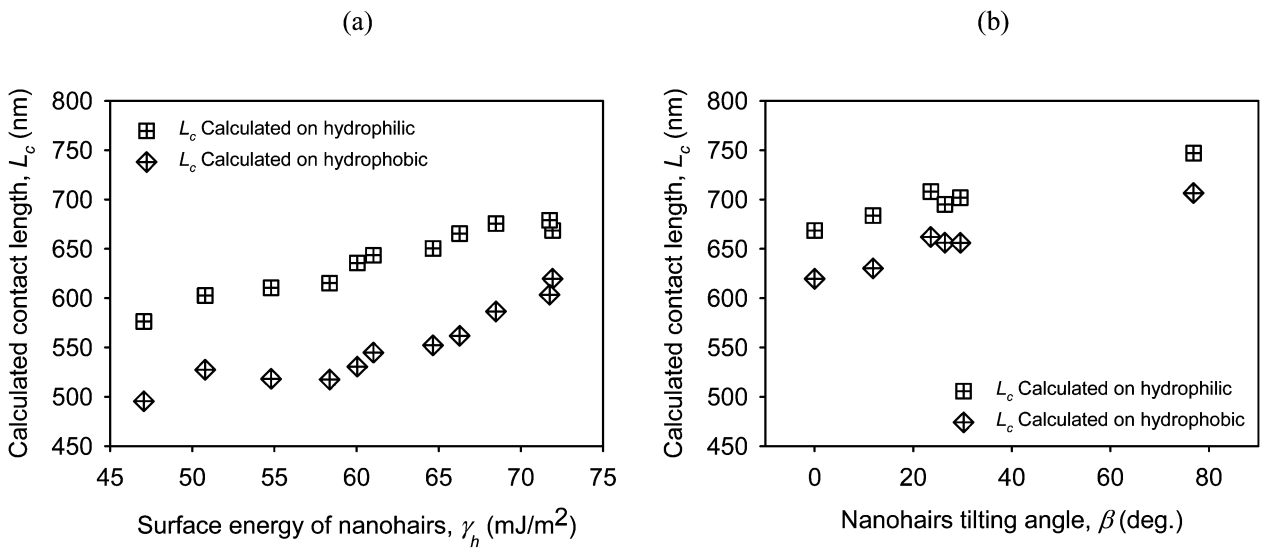

Fig. 4 The estimated contact length, L_c, as a function of surface energy (a) and tilting angle (b) of nanohairs.

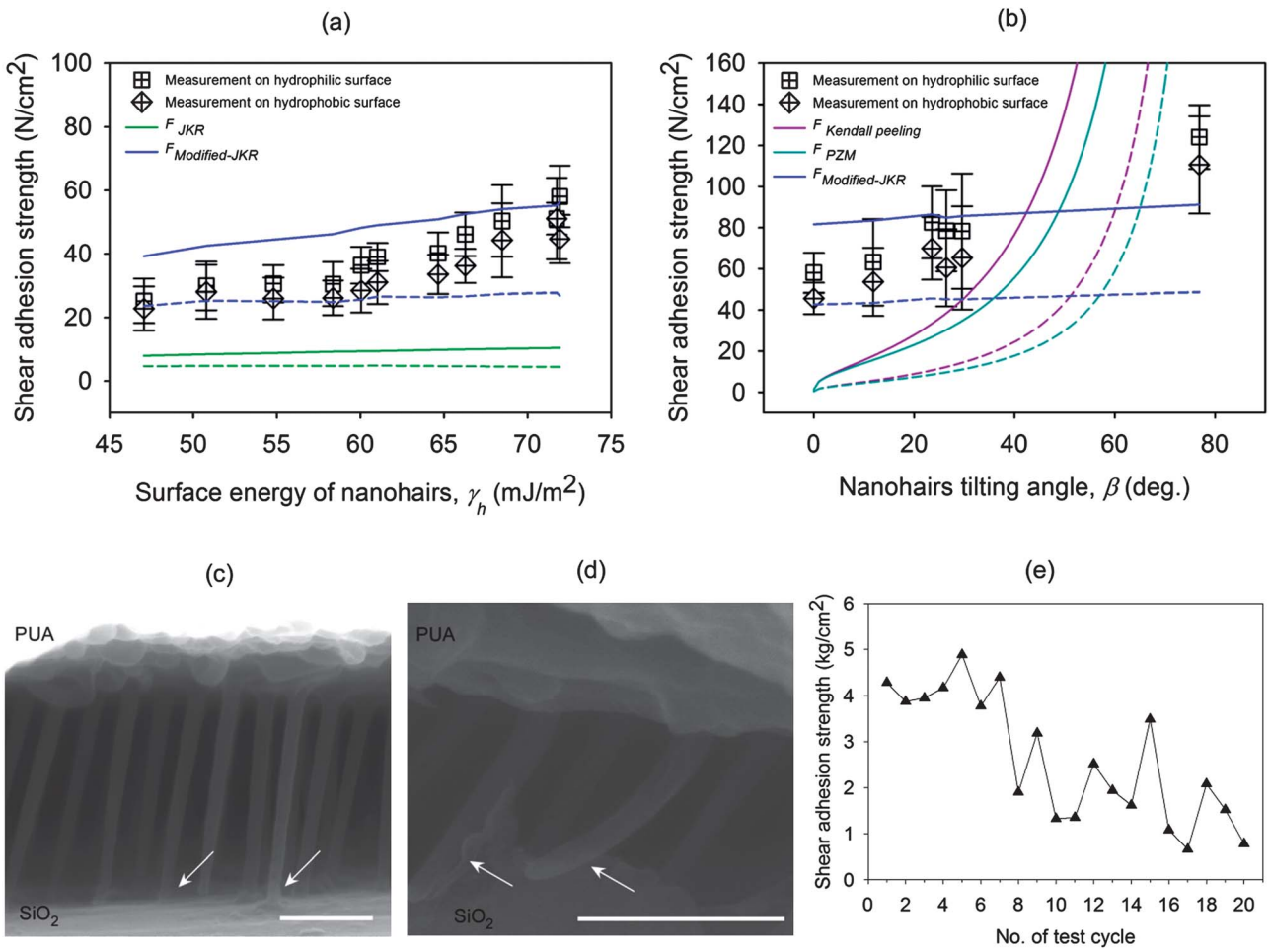

Fig. 5 (a and b) Comparison of the measured adhesion strength on hydrophilic and hydrophobic surfaces with the theoretical predictions on vertical nanohairs with variation of surface energy (a) and tilted nanohairs with variation of tilting angle (b). The solid lines are for the calculations of adhesion strength on hydrophilic surfaces and the dashed lines on hydrophobic surfaces. Note that for all variations, the modified-JKR model for side contact is highly matched with the experimental measurement. The SEM images for the initial contacts between vertical and tilted nanohairs are shown in (c) and (d), respectively, with the bars shown at 500 nm. The arrows in (c) and (d) indicate the locations of contact at the contacting surface. An example of the adhesion strength test cycle of a vertical nanohair sample after aging for 5 days is shown in (e). Note that the adhesion strength is well maintained up to 7 times.

As shown in Fig. 5(b), the adhesion strength was increased significantly from 58.1 to 124.1 N cm^{-2} and from 45.7 to 110.6 N cm^{-2} on hydrophilic and hydrophobic counter surfaces, respectively, indicating a more than two-fold increase by simply modulating the tilting angle of the nanohairy structure. For comparison, the value is still lower than the theoretical maximum adhesion strength of gecko foot hairs (~325 N cm^{-2}),[2,3] which appears to be ascribed to the smaller hair density of the current system (6.16×10^8 hairs cm^{-2}) compared to that of real gecko hairs ($\sim 1.625 \times 10^9$ spatula cm^{-2}).

As shown in the plots, the theoretical adhesion strength using the modified-JKR shows better agreement with the experimental results (Fig. 5(b)) as compared to Kendall peeling and PZ models. A slight overestimation in the side contact model at a lower tilting angle ($\beta < 40°$) indicates that the actual number of nanohairs in side contact could be lower than estimated due to possible damage of nanohairs during fabrication, non-uniform contact by a preload, and roughness of the counter surface. Also, an underestimation at higher tilting angle ($\beta > 60°$) reveals that the actual contact number is higher, which is probably associated with the unique bending geometry of hairs. Namely, only the tip part is stooped for higher tilting angle as compared to straight hairs (see Fig. 2), so that the size contact would be more enhanced. The SEM images of the initial contact after applying a preload for the vertical and tilted nanohairs are shown in Fig. 5 (c) and (d), respectively. Here, it is clear that the pre-load does not affect the initial contact of nanohairs. However, further bending can be made in the course of the dynamic application of shear force, resulting in the enhanced contact length close to the theoretical contact length. In Fig. 5(e) we present an example of the durability of the vertical nanohairs. As shown, the treated nanohairs can maintain the adhesion strength up to 7 times and the strength becomes deteriorated for further test.

Conclusion

We have presented the effects of surface energy and tilting angle of nanohairs on the shear adhesion strength. By utilizing Ar ion beam irradiation, geometry-controllable high aspect-ratio nanohairs (100 nm diameter and 1 μm height) were prepared with

various tilting angles ranging from 0° (straight) to 75° (stooped nanohairs). Subsequent O_2 ion beam treatment was capable of transforming the as-prepared hydrophobic hairy surface into hydrophilic, accompanying a significant rise in the shear adhesion force (maximum adhesion of 124.1 N cm^{-2} on a hydrophilic counter surface). From the measurement with the variation of surface energy on tilted nanohairs, the macroscopic shear adhesion force heavily relied on the tilting angle of nanohairs, showing a more than two-fold increase as the tilted angle was increased from 0° to 75°. Based on these results, one can engineer dry adhesion strength by modulating the intrinsic surface energy and tilting angle of nanohairs. Moreover, the current method allows for large-area fabrication in a more rapid and scalable manner, providing an efficient route to the preparation of directional, dry adhesive surfaces.

Acknowledgements

This work was supported by the KIST (2E22200), and a grant (06K1501-01610) from the Global Excellent Technology Innovation R&D Program funded by the Ministry of Knowledge Economy in Korea. This work was also supported in part by Basic Science Research Program (2010-0027955), World Class University (WCU) Program (R31-2008-000-10083-0) funded by the Ministry of Education, Science and Technology (MEST), Institute of Advanced Machinery and Design (IAMD) and Engineering Research Institute of Seoul National University.

Notes and references

1 R. Ruibal and V. Ernst, *J. Morphol.*, 1965, **117**, 271–294.
2 D. J. Irschick, C. C. Austin, K. Petren, R. N. Fisher, J. B. Losos and O. Ellers, *Biol. J. Linn. Soc.*, 1996, **59**, 21–35.
3 K. Autumn and W. Hansen, *J. Comp. Physiol., A*, 2006, **192**, 1205–1212.
4 K. Autumn, M. Sitti, Y. C. A. Liang, A. M. Peattie, W. R. Hansen, S. Sponberg, T. W. Kenny, R. Fearing, J. N. Israelachvili and R. J. Full, *Proc. Natl. Acad. Sci. U. S. A.*, 2002, **99**, 12252–12256.
5 G. Huber, H. Mantz, R. Spolenak, K. Mecke, K. Jacobs, S. N. Gorb and E. Arzt, *Proc. Natl. Acad. Sci. U. S. A.*, 2005, **102**, 16293–16296.
6 K. Autumn, Y. A. Liang, S. T. Hsieh, W. Zesch, W. P. Chan, T. W. Kenny, R. Fearing and R. J. Full, *Nature*, 2000, **405**, 681–685.
7 M. K. Kwak, H. E. Jeong, T. I. Kim, H. Yoon and K. Y. Suh, *Soft Matter*, 2010, **6**, 1849–1857.
8 S. Vajpayee, K. Khare, S. Yang, C.-Y. Hui and A. Jagota, *Adv. Funct. Mater.*, 2011, **21**, 547–555.
9 M. P. Murphy, B. Aksak and M. Sitti, *Small*, 2009, **5**, 170–175.
10 A. del Campo, C. Greiner, I. Alvarez and E. Arzt, *Adv. Mater.*, 2007, **19**, 1973–1977.
11 C. Greiner, A. del Campo and E. Arzt, *Langmuir*, 2007, **23**, 3495–3502.
12 B. Aksak, M. P. Murphy and M. Sitti, *Langmuir*, 2007, **23**, 3322–3332.
13 N. E. Stork, *J. Exp. Biol.*, 1980, **88**, 91–108.
14 W. K. Cho and I. S. Choi, *Adv. Funct. Mater.*, 2008, **18**, 1089–1096.
15 H. Ko, Z. X. Zhang, J. C. Ho, K. Takei, R. Kapadia, Y. L. Chueh, W. Z. Cao, B. A. Cruden and A. Javey, *Small*, 2010, **6**, 22–26.
16 M. K. Kwak, H. E. Jeong, W. G. Bae, H. S. Jung and K. Y. Suh, *Small*, 2011, **7**, 2266–2300.
17 P. H. Niewiarowski, S. Lopez, L. Ge, E. Hagan and A. Dhinojwala, *PLoS One*, 2008, **3**, e2192.
18 M. Fuji, K. Machida, T. Takei, T. Watanabe and M. Chikazawa, *Langmuir*, 1999, **15**, 4584–4589.
19 T. W. Kim and B. Bhushan, *J. R. Soc. Interface*, 2008, **5**, 319–327.
20 H. Ko, Z. X. Zhang, Y. L. Chueh, J. C. Ho, J. Lee, R. S. Fearing and A. Javey, *Adv. Funct. Mater.*, 2009, **19**, 3098–3102.
21 D. Chandra and S. Yang, *Acc. Chem. Res.*, 2010, **43**, 1080–1091.
22 B. Pokroy, S. H. Kang, L. Mahadevan and J. Aizenberg, *Science*, 2009, **323**, 237–240.
23 H. E. Jeong, J. K. Lee, H. N. Kim, S. H. Moon and K. Y. Suh, *Proc. Natl. Acad. Sci. U. S. A.*, 2009, **106**, 5639–5644.
24 H. E. Jeong and K. Y. Suh, *Nano Today*, 2009, **4**, 335–346.
25 C. W. Tsao, L. Hromada, J. Liu, P. Kumar and D. L. DeVoe, *Lab Chip*, 2007, **7**, 499–505.
26 D. Pasquariello, M. Lindeberg, C. Hedlund and K. Hjort, *Sens. Actuators, A*, 2000, **82**, 239–244.
27 T. I. Kim, H. E. Jeong, K. Y. Suh and H. H. Lee, *Adv. Mater.*, 2009, **21**, 2276–2281.
28 T. I. Kim and K. Y. Suh, *Soft Matter*, 2009, **5**, 4131–4135.
29 M. Morra, E. Occhiello, R. Marola, F. Garbassi, P. Humphrey and D. Johnson, *J. Colloid Interface Sci.*, 1990, **137**, 11–24.
30 Y. Rahmawan, M. W. Moon, K. S. Kim, K. R. Lee and K. Y. Suh, *Langmuir*, 2010, **26**, 484–491.
31 T. G. Cha, J. W. Yi, M. W. Moon, K. R. Lee and H. Y. Kim, *Langmuir*, 2010, **26**, 8319–8326.
32 M. W. Moon, T. G. Cha, K. R. Lee, A. Vaziri and H. Y. Kim, *Soft Matter*, 2010, **6**, 3924–3929.
33 S. F. Ahmed, M. W. Moon, C. Kim, Y. J. Jang, S. Han, J. Y. Choi, W. W. Park and K. R. Lee, *Appl. Phys. Lett.*, 2010, **97**, 081908.
34 D. K. Owens and R. C. Wendt, *J. Appl. Polym. Sci.*, 1969, **13**, 1741.
35 M. W. Moon and A. Vaziri, *Scr. Mater.*, 2009, **60**, 44–47.
36 J. W. Yi, M. W. Moon, S. F. Ahmed, H. Kim, T. G. Cha, H. Y. Kim, S. S. Kim and K. R. Lee, *Langmuir*, 2010, **26**, 17203–17209.
37 R. K. Roy, H. W. Choi, J. W. Yi, M. W. Moon, K. R. Lee, D. K. Han, J. H. Shin, A. Kamijo and T. Hasebe, *Acta Biomater.*, 2009, **5**, 249–256.
38 M. Zenkiewicz, *Polym. Test.*, 2007, **26**, 14–19.
39 C. J. van Oss, R. J. Good and M. K. Chaudhury, *J. Colloid Interface Sci.*, 1986, **111**, 378–390.
40 F. M. Fowkes, *J. Phys. Chem.*, 1963, **67**, 2538–2541.
41 S. Wu, *J. Adhes.*, 1973, **5**, 39–55.
42 N. J. Glassmaker, A. Jagota, C. Y. Hui and J. Kim, *J. R. Soc. Interface*, 2004, **1**, 23–33.
43 K. L. Johnson, K. Kendall and A. D. Roberts, *Proc. R. Soc. London, Ser. A*, 1971, **324**, 301–313.
44 M. K. Chaudhury, T. Weaver, C. Y. Hui and E. J. Kramer, *J. Appl. Phys.*, 1996, **80**, 30–37.
45 J. Lee, C. Majidi, B. Schubert and R. S. Fearing, *J. R. Soc. Interface*, 2008, **5**, 835–844.
46 C. Majidi, *Mech. Res. Commun.*, 2009, **36**, 369–372.
47 C. S. Majidi, R. E. Groff and R. S. Fearing, *J. Appl. Phys.*, 2005, **98**, 103521.
48 H. E. Jeong, J. K. Lee, M. K. Kwak, S. H. Moon and K. Y. Suh, *Appl. Phys. Lett.*, 2010, **96**, 043704.
49 K. Kendall, *J. Phys. D: Appl. Phys.*, 1975, **8**, 1449.
50 M. Varenberg, N. M. Pugno and S. N. Gorb, *Soft Matter*, 2010, **6**, 3269.
51 N. S. Pesika, Y. Tian, B. X. Zhao, K. Rosenberg, H. B. Zeng, P. McGuiggan, K. Autumn and J. N. Israelachvili, *J. Adhes.*, 2007, **83**, 383–401.
52 K. Autumn, C. Majidi, R. E. Groff, A. Dittmore and R. Fearing, *J. Exp. Biol.*, 2006, **209**, 3558–3568.

